Editors' Suggestion | Featured in Physics

Proton Mass Decomposition from the QCD Energy Momentum Tensor

Yi-Bo Yang,[1,5] Jian Liang,[2] Yu-Jiang Bi,[3] Ying Chen,[3,4] Terrence Draper,[2] Keh-Fei Liu,[2] and Zhaofeng Liu[3,4]
[1]*Department of Physics and Astronomy, Michigan State University, East Lansing, Michigan 48824, USA*
[2]*Department of Physics and Astronomy, University of Kentucky, Lexington, Kentucky 40506, USA*
[3]*Institute of High Energy Physics, Chinese Academy of Sciences, Beijing 100049, China*
[4]*School of Physics, University of Chinese Academy of Sciences, Beijing 100049, China*
[5]*Institute of Theoretical Physics, Chinese Academy of Sciences, Beijing 100190, China*

(Received 4 September 2018; published 19 November 2018)

We report results on the proton mass decomposition and also on related quark and glue momentum fractions. The results are based on overlap valence fermions on four ensembles of $N_f = 2 + 1$ domain wall fermion configurations with three lattice spacings and three volumes, and several pion masses including the physical pion mass. With fully nonperturbative renormalization (and universal normalization on both quark and gluon), we find that the quark energy and glue field energy contribute 32(4)(4)% and 36(5)(4)% respectively in the $\overline{\text{MS}}$ (modified minimal substraction) scheme at $\mu = 2$ GeV. A quarter of the trace anomaly gives a 23(1)(1)% contribution to the proton mass based on the sum rule, given 9(2)(1)% contribution from the u, d, and s quark scalar condensates. The u, d, s, and glue momentum fractions in the $\overline{\text{MS}}$ scheme are in good agreement with global analyses at $\mu = 2$ GeV.

DOI: 10.1103/PhysRevLett.121.212001

Introduction.—In the standard model, the Higgs boson provides the origin of quark masses. But how it is related to the proton mass and thus the masses of nuclei and atoms is another question. The masses of the valence quarks in the proton are just ~3 MeV per quark, which is directly related to the Higgs boson, while the total proton mass is 938 MeV. The percentages of the quark and gluon contributions to the proton mass can only be provided by solving QCD nonperturbatively and/or with information from experiment. With phenomenological input, the first decomposition was carried out by Ji [1]. As in Refs. [1,2], the Hamiltonian of QCD can be decomposed as

$$M = -\langle T_{44}\rangle = \langle H_m\rangle + \langle H_E\rangle(\mu) + \langle H_g\rangle(\mu) + \frac{1}{4}\langle H_a\rangle, \quad (1)$$

in the rest frame of the hadron state where M is the hadron mass, and

$$T_{\mu\nu} = \frac{1}{4}\overline{\psi}\gamma_{(\mu}\overleftrightarrow{D}_{\nu)}\psi + F_{\mu\alpha}F_{\nu\alpha} - \frac{1}{4}\delta_{\mu\nu}F^2 \quad (2)$$

is the energy momentum tensor (EMT) of QCD in Euclidean space [3] with $\langle T_{44}\rangle$ as its expectation value in the hadron, and the trace anomaly gives the following:

$$M = -\langle T_{\mu\mu}\rangle = \langle H_m\rangle + \langle H_a\rangle. \quad (3)$$

The H_m, H_E, and H_g in the above equations denote the contributions from the quark condensate, the quark energy, and the glue field energy, respectively:

$$H_m = \sum_{u,d,s\cdots}\int d^3x m\overline{\psi}\psi,$$
$$H_E = \sum_{u,d,s\cdots}\int d^3x\overline{\psi}(\vec{D}\cdot\vec{\gamma})\psi,$$
$$H_g = \int d^3x\frac{1}{2}(B^2 - E^2). \quad (4)$$

The QCD anomaly term H_a is the joint contribution from the quantum anomalies of both glue and quark,

$$H_a = H_g^a + H_m^\gamma,$$
$$H_g^a = \int d^3x\frac{-\beta(g)}{g}(E^2 + B^2),$$
$$H_m^\gamma = \sum_{u,d,s\cdots}\int d^3x\gamma_m m\overline{\psi}\psi. \quad (5)$$

All the $\langle H\rangle$ are defined by $\langle N|H|N\rangle/\langle N|N\rangle$ where $|N\rangle$ is the nucleon state in the rest frame. Note that $\langle H_E + H_g\rangle$, $\langle H_m\rangle$ and $\langle H_a\rangle$ are scale and renormalization scheme independent, but $\langle H_E\rangle(\mu)$ and $\langle H_g\rangle(\mu)$ separately have scale and scheme dependence.

The nucleon mass M can be calculated from the nucleon two-point function. If one calculates further $\langle H_m \rangle$ and $\langle H_E \rangle(\mu)$, then $\langle H_g \rangle(\mu)$ and $\langle H_a \rangle$ can be obtained through Eqs. (1) and (3). The approach has been adopted to decompose S-wave meson masses, from light mesons to charmoniums, to gain insight about contributions of each term [2]. But the mixing between $\langle H_E \rangle(\mu)$ and $\langle H_m \rangle$ will be nontrivial under the lattice regularization when there is any breaking of the quark equation of motion at finite spacing. On the other hand, if we obtain the renormalized quark momentum fraction $\langle x \rangle_q^R$ in the continuum limit, and define the renormalized quark energy $\langle H_E^R \rangle$ in term of $\langle x \rangle_q^R$ and $\langle H_m \rangle$ with the help of the equation of motion, i.e.,

$$\langle H_E^R \rangle = \frac{3}{4} \langle x \rangle_q^R M - \frac{3}{4} \langle H_m \rangle, \tag{6}$$

then the additional mixing can be avoided. Similarly, the renormalized glue field energy can be accessed from the glue momentum fraction $\langle x \rangle_g^R$ by

$$\langle H_g^R \rangle = \frac{3}{4} \langle x \rangle_g^R M. \tag{7}$$

In the present Letter, we use the lattice derivative operator for the quark EMT and a combination of plaquettes for the gauge EMT and address their normalization in addition to renormalization and mixing. We calculate the proton mass and the renormalized $\langle x \rangle_{q,g}$ on four lattice ensembles, and extrapolate the results to the physical pion mass with a global fit including finite lattice spacing and volume corrections. Then we combine previously calculated $\langle H_m \rangle$ [4] to obtain $\langle H_a \rangle$ from Eq. (3), and the full decomposition of the proton energy in the rest frame as shown in Eq. (1).

Numerical setup.—We use overlap valence fermions on $(2+1)$ flavor RBC/UKQCD domain wall fermion gauge configurations from four ensembles on $24^3 \times 64$ (24I), $32^3 \times 64$ (32I) [5], $32^3 \times 64$ (32ID), and $48^3 \times 96$ (48I) [6] lattices. These ensembles cover three values of the lattice spacing and volume respectively, and four values of the quark mass in the sea, which allows us to implement a global fit on our results to control the systematic uncertainties as in Ref. [4,7]. Other parameters of the ensembles used are listed in Table I.

The effective quark propagator of the massive overlap fermion is the inverse of the operator $(D_c + m)$ [8,9], where D_c is chiral, i.e., $\{D_c, \gamma_5\} = 0$ [10], and its detailed definition can be found in our previous work [11–13]. We used four quark masses from the range $m_\pi \in (250, 400)$ MeV on the 24I and 32I ensembles, and six or five quark masses from $m_\pi \in (140, 400)$ MeV on the 48I/32ID ensembles respectively, which have larger volumes and thus allow a lighter pion mass with the constraint $m_\pi L > 3.8$. One step of the hypercubic (HYP) smearing [14] is applied on all the configurations to improve the signal. Numerical details regarding the calculation of the overlap operator, eigenmode deflation for the inversion of the quark matrix, and the Z_3 grid smeared sources with low-mode substitution (LMS) to increase statistics are given in Refs. [11–13,15].

TABLE I. The parameters for the RBC/UKQCD configurations [6]: spatial and temporal size, lattice spacing, sea strange quark mass under $\overline{\text{MS}}$ scheme at 2 GeV, pion mass with the degenerate light sea quark, and the number of configurations.

Symbol	$L^3 \times T$	a (fm)	$m_s^{(s)}$ (MeV)	m_π (MeV)	N_{cfg}
32ID	$32^3 \times 64$	0.1431(7)	89.4	171	200
24I	$24^3 \times 64$	0.1105(3)	120	330	203
48I	$48^3 \times 96$	0.1141(2)	94.9	139	81
32I	$32^3 \times 64$	0.0828(3)	110	300	309

Proton mass.—We first calculate the proton mass on these four ensembles and apply the SU(4|2) mixed action HBχPT functional form [16] to fit the results,

$$\begin{aligned} M(m_\pi^v, m_\pi^{\text{sea}}, a, L) = {} & M_0 + C_1 (m_\pi^v)^2 + C_2 (m_\pi^{\text{sea}})^2 \\ & - \frac{(g_A^2 - 4 g_A g_1 - 5 g_1^2)\pi}{3(4\pi f_\pi)^2} (m_\pi^v)^3 \\ & - \frac{(8 g_A^2 + 4 g_A g_1 + 5 g_1^2)\pi}{3(4\pi f_\pi)^2} (m_\pi^{pq})^3 \\ & + C_3^{I/ID} a^2 + C_4 \frac{(m_\pi^v)^2}{L} e^{-m_\pi^v L}, \end{aligned} \tag{8}$$

where M_0, $C_{1,2,3,4}$, the axial vector coupling g_A, and an additional partially quenched one g_1 are free parameters; $f_\pi = 0.122(9)$ GeV is the pion decay constant; $m_\pi^{v,\text{sea}}$ is the valence and sea pion mass, respectively; $m_\pi^{pq} = \sqrt{(m_\pi^v)^2 + (m_\pi^{\text{sea}})^2 + \Delta_{\text{mix}} a^2}$ is the partially quenched mass with the mixed action term $\Delta_{\text{mix}} a^2$; and a is the lattice spacing. The $\mathcal{O}(m_\pi^3)$ logarithm function $\mathcal{F}$ in the original functional form is dropped since it turns out to be not useful to constrain the fit. Note that we used C_3^I for the 24I/48I/32I ensembles and C_3^{ID} for 32ID ensemble as they used different gauge actions. We get the prediction of the proton mass at the physical point as $M(m_\pi^{\text{phys}}, m_\pi^{\text{phys}}, 0, \infty) = 0.960(13)$ GeV with $\chi^2/\text{d.o.f.} = 0.52$. From the fit, we can also get the light quark mass sigma term $H_{m,u+d} \simeq (\partial M/\partial m_\pi) m_\pi/2 = 52(8)$ MeV, which is consistent with our previous direct calculation 46(7)(2) MeV [4]. The g_A we get from the fit is 0.9(2) which is consistent with the experimental result 1.2723(23) [17] within 2σ. Alternatively, using the experimental value of g_A predicts the proton mass as 0.931(8) with a χ^2/d.o.f. of 1.5. The results of the proton mass with the partially quenching effect ($m_\pi^{\text{sea}} \neq m_\pi^v$) subtracted are plotted in Fig. 1 as a function of the valence pion mass, together with the blue band for our prediction in the continuum limit. The difference between

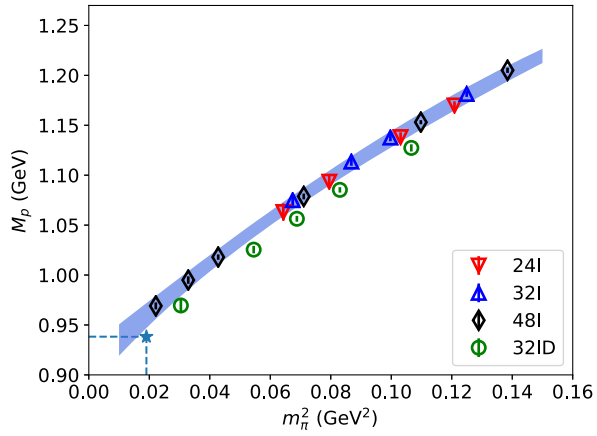

FIG. 1. The proton mass as a function of the pion mass at different lattice spacings and volumes, after partially quenching effects are subtracted. The star shows the physical proton mass.

the results with different symbols reflects the discretization errors and finite volume effects, which are reasonably small, as shown in Fig. 1.

Momentum fraction.—The quark and gluon momentum fractions in the nucleon can be defined by the traceless diagonal part of the EMT matrix element in the rest frame [18],

$$\langle x\rangle_{q,g} \equiv -\frac{\langle N|\frac{4}{3}\overline{T}^{q,g}_{44}|N\rangle}{M\langle N|N\rangle},$$
$$\overline{T}^{q}_{44} = \int d^3x\overline{\psi}(x)\frac{1}{2}\left(\gamma_4\overleftrightarrow{D}_4 - \frac{1}{4}\sum_{i=0,1,2,3}\gamma_i\overleftrightarrow{D}_i\right)\psi(x),$$
$$\overline{T}^{g}_{44} = \int d^3x\frac{1}{2}[E(x)^2 - B(x)^2]. \tag{9}$$

In practice, we calculated ratios of the three-point function to the two-point function

$$R^{q,g}(t_f,t) = \frac{\langle 0|\int d^3y\Gamma^e\chi_S(\vec{y},t_f)\overline{T}^{q,g}_{44}(t)\sum_{\vec{x}\in G}\overline{\chi}_S(\vec{x},0)|0\rangle}{\langle 0|\int d^3y\Gamma^e\chi_S(\vec{y},t_f)\sum_{\vec{x}\in G}\overline{\chi}_S(\vec{x},0)|0\rangle}, \tag{10}$$

where χ_S is the standard proton interpolation field with Gaussian smearing applied to all three quarks, and Γ^e is the unpolarized projection operator of the nucleon. All the correlation functions from the source points $\vec{x}$ in the grid G are combined to improve the signal-to-noise ratio (SNR) [13]. When t_f is large enough, $R^{q,g}(t_f,t)$ approaches the bare nucleon matrix element $\langle N|\overline{T}^{q,g}_{44}|N\rangle$.

For each quark mass on each ensemble, we construct $R(t_f,t)$ for several sink-source separations t_f from 0.7 fm to 1.5 fm and all the current insertion times t between the source and sink, combine all the data to do the two-state fit, and then obtain the matrix elements we want with the excited-states contamination removed properly. The more detailed discussion of the simulation setup and the two-state fit can be found in our previous work [4,7,19].

To improve the signal in the disconnected insertion part of $\langle x\rangle_{q,g}$, all the time slices are looped over for the proton propagator. For $\langle x\rangle_g$, the cluster-decomposition error reduction (CDER) technique is applied, as described in Refs. [20,21].

The renormalized momentum fractions $\langle x\rangle^R$ in the $\overline{\text{MS}}$ scheme at scale μ are

$$\langle x\rangle^R_{u,d,s} = Z^{\overline{\text{MS}}}_{QQ}(\mu)\langle x\rangle_{u,d,s} + \delta Z^{\overline{\text{MS}}}_{QQ}(\mu)\sum_{q=u,d,s}\langle x\rangle_q + Z^{\overline{\text{MS}}}_{QG}(\mu)\langle x\rangle_g,$$
$$\langle x\rangle^R_g = Z^{\overline{\text{MS}}}_{GQ}(\mu)\sum_{q=u,d,s}\langle x\rangle_q + Z^{\overline{\text{MS}}}_{GG}\langle x\rangle_g, \tag{11}$$

where $\langle x\rangle_{u,d,s,g}$ is the bare momentum fraction under the lattice regularization, and the renormalization constants in the $\overline{\text{MS}}$ at scale μ are defined through the RI/MOM scheme

$$\begin{pmatrix} Z^{\overline{\text{MS}}}_{QQ}(\mu) + N_f\delta Z^{\overline{\text{MS}}}_{QQ}(\mu) & N_f Z^{\overline{\text{MS}}}_{QG}(\mu) \\ Z^{\overline{\text{MS}}}_{GQ}(\mu) & Z^{\overline{\text{MS}}}_{GG}(\mu)\end{pmatrix}$$
$$\equiv \left\{\left[\begin{pmatrix} Z_{QQ}(\mu_R) + N_f\delta Z_{QQ} & N_f Z_{QG}(\mu_R) \\ Z_{GQ}(\mu_R) & Z_{GG}(\mu_R)\end{pmatrix} \times \begin{pmatrix} R_{QQ}(\frac{\mu}{\mu_R}) + \mathcal{O}(N_f\alpha_s^2) & N_f R_{QG}(\frac{\mu}{\mu_R}) \\ R_{GQ}(\frac{\mu}{\mu_R}) & R_{GG}(\frac{\mu}{\mu_R})\end{pmatrix}\right]|_{a^2\mu_R^2\to 0}\right\}^{-1} \tag{12}$$

and $Z_{QQ}(\mu) = [(Z_{QQ}(\mu_R)R_{QQ}(\mu/\mu_R))|_{a^2\mu_R^2\to 0}]^{-1}$. Note that the isovector matching coefficient $R_{QQ}(\mu/\mu_R)$ has been obtained at the three-loop level [22] while just the one-loop level results of the other R s are available [23].

We list the renormalization constants for $\overline{T}^{q,g}_{44}$ at $\overline{\text{MS}}$ 2 GeV in Table II and the details of the nonperturbative renormalization (NPR) calculation are discussed in the Supplementary Material [24], based on the previous research of Refs. [25–27].

After the renormalization, the total momentum fraction is generally larger than 1 by 20–30% on the four ensembles due to the discretization error. We apply a uniform normalization on both the quark and glue momentum fractions at each quark mass of each ensemble, and plot these normalization factors $\overline{Z} = \langle x\rangle^{-1}_{u+d+s+g}$ in the lower-right panel of Fig. 2. $\overline{Z}$ should approach unity as can be seen by comparing the normalization of the 24I ($a = 0.1105$ fm) and the 32I ($a = 0.0828$ fm) lattices, which have about the same quark mass, for $m_\pi^2 > 0.08$ GeV^2.

Then the pion mass dependence of the renormalized and normalized $\langle x\rangle^R_{u,d,s,g}$ are fitted with the following empirical form simultaneously,

$$\langle x\rangle^R(m_\pi^v, m_\pi^{\text{sea}}, a, L) = \langle x\rangle^R_0 + D_1[(m_\pi^v)^2 - (m_\pi^0)^2] + D_2[(m_\pi^v)^2 - (m_\pi^{\text{sea}})^2] + D_3^{I/ID}a^2 + D_4e^{-m_\pi^v L}, \tag{13}$$

TABLE II. The nonperturbative renormalization (NPR) constants on different ensembles, at $\overline{\text{MS}}$ 2 GeV. The 24I and 48I ensembles have the same lattice spacing and thus share the renormalization constants. The two uncertainties are the statistical and systematic ones, respectively, with the details provided in the Supplementary Material [24].

Symbol	Z_{QQ}	δZ_{QQ}	Z_{QG}	Z_{GQ}	Z_{GG}
32ID	1.25(0)(2)	0.018(2)(2)	0.017(17)	0.57(3)(6)	1.29(5)(9)
24I/48I	1.24(0)(2)	0.012(2)(2)	0.007(14)	0.35(3)(6)	1.07(4)(4)
32I	1.25(0)(2)	0.008(2)(2)	0.000(14)	0.18(2)(2)	1.10(4)(5)

and the χ^2/d.o.f. is 0.20. Our prediction of the $\langle x\rangle^R_{u,d,s,g}$ are 0.307(30)(18), 0.160(27)(40), 0.051(26)(5), and 0.482(69)(48), respectively, where the first error is the statistical one and the second error includes the systematic uncertainties from the chiral, continuum, and infinite volume interpolation or extrapolation. The systematic uncertainties from the two-state fit and CDER for $\langle x\rangle_g$ haven't been taken into account yet and will be investigated in the future. With the normalization factors shown in lower-right panel of Fig. 2, all the predictions of the momentum fractions are consistent with the phenomenological global fit at $\overline{\text{MS}}$ 2 GeV, e.g., CT14 [28] values $\langle x\rangle^R_u = 0.348(3)$, $\langle x\rangle^R_d = 0.190(3)$, $\langle x\rangle^R_s = 0.035(5)$, and $\langle x\rangle^R_g = 0.416(5)$. The other global fits results [29–33], summarized in Ref. [34], are consistent with CT14. After the partially quenching effect term proportional to D_2 is subtracted, the $\langle x\rangle^R_{u,d,s,g}$ at different ensembles and valence quark masses are illustrated in Fig. 2 as a function of m_π^2, in the upper-left panel for the u and d cases and the upper-right panel for the s and g cases. The bands on the figures show our predictions in the continuum limit with their uncertainties (blue for the statistics and cyan for the total).

We also predict the isovector momentum fraction $\langle x\rangle^R_{u-d}$ as 0.151(28)(29), which is consistent with the CT14 result 0.158(6) [28], in the lower-left panel of Fig. 2.

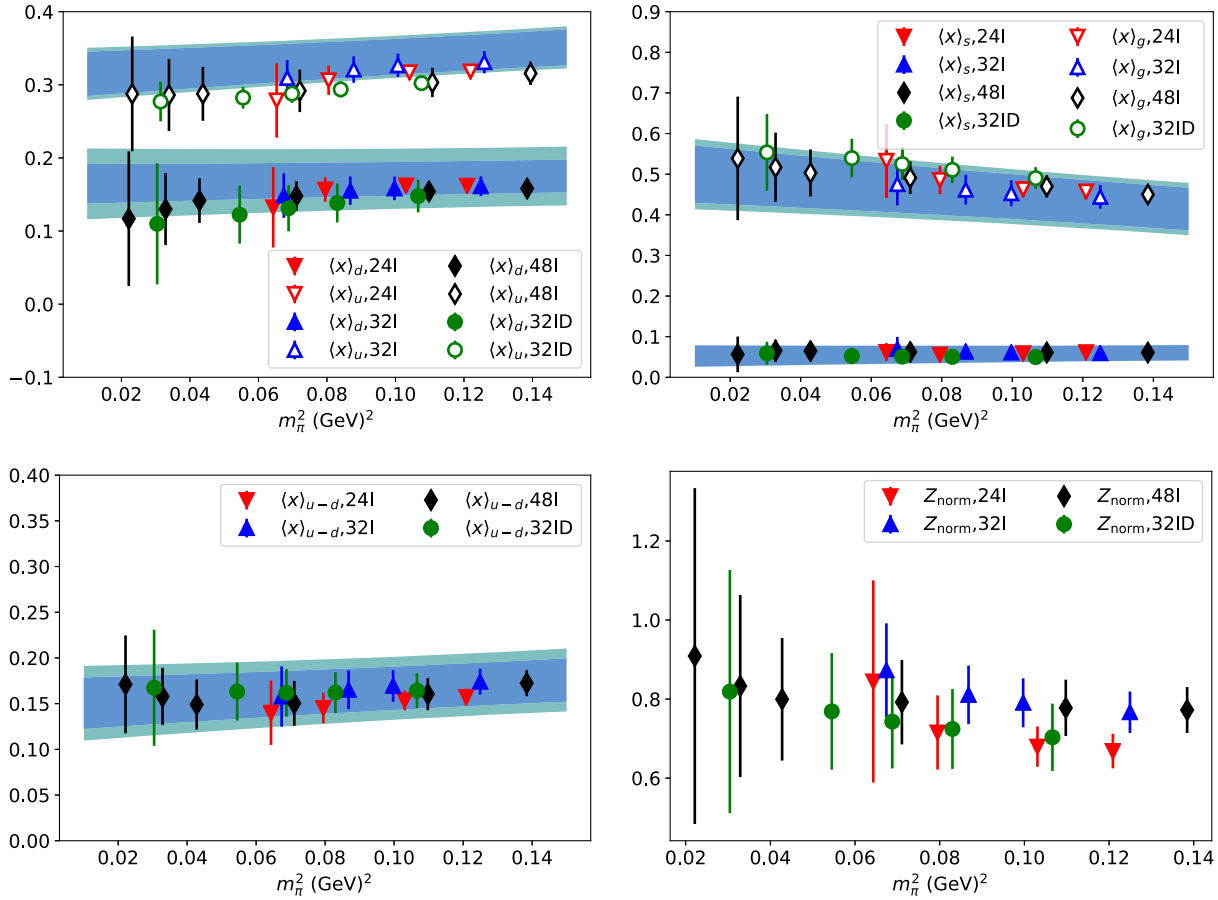

FIG. 2. The momentum fractions of different quark flavors and glue in the proton, at $\overline{\text{MS}}$ 2 GeV. The two upper panels show the u, d, s, and g momentum fractions, respectively, and two lower ones show the u–d case (left panel), and also the normalization factors for the momentum fraction sum rule (right panel). The bands on the figures show our predictions in the continuum limit of the momentum fractions with their statistical (blue) and total (cyan) uncertainties. The data points correspond to our simulation results at different valence quark masses on different ensembles, with the partially quenching effect subtracted.

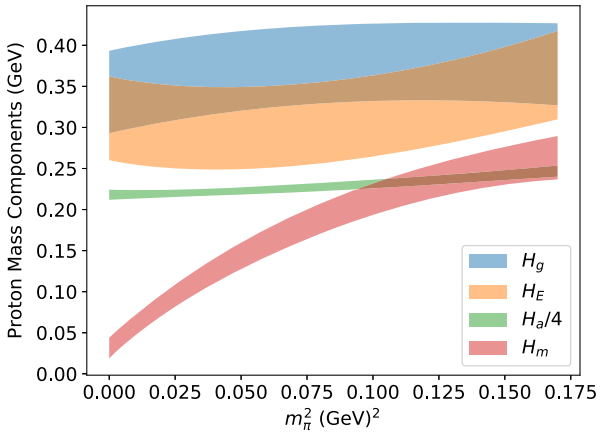

FIG. 3. The valence pion mass dependence of the proton mass decomposition in terms of the quark condensate $\langle H_m \rangle$, quark energy $\langle H_E \rangle$, glue field energy $\langle H_g \rangle$, and trace anomaly $\langle H_a \rangle/4$.

Final proton mass decomposition.—With these momentum fractions at $\overline{\text{MS}}$ 2 GeV, we can apply Eqs. (6) and (7) to obtain the quark and glue energy contributions in the proton mass (or more precisely, the proton energy in the rest frame). Combined with the quark scalar condensate and trace anomaly contributions, the entire proton mass decomposition is illustrated in Fig. 3 as a function of the valence pion mass. As shown in the figure, the major quark mass dependence comes from the quark condensate term, and the other components are almost independent of the quark mass. At the physical point, the quark and glue energy contributions are 32(4)(4)% and 36(5)(4)% respectively. With the quark scalar condensate contribution of 9(2)(1)% [4], we can obtain that a quarter of the trace anomaly contributes 23(1)(1)% with $N_f = 2 + 1$.

In summary, we present a simulation strategy to calculate the proton mass decomposition. The renormalization and mixing between the quark and glue energy can be calculated nonperturbatively, and the quark scalar condensate contribution and the trace anomaly are renormalization group invariant. Based on this strategy, the lattice simulation is carried out on four ensembles with three lattice spacings and volumes, and several pion masses, including the physical pion mass, to control the respective systematic uncertainties. With nonperturbative renormalization and normalization, the individual u, d, s, and glue momentum fractions agree with those from the global fit in the $\overline{\text{MS}}$ scheme at 2 GeV. Quark energy, gluon energy, and quantum anomaly contributions to the proton mass are fairly insensitive to the pion mass up to 400 MeV within our statistical and systematic uncertainties.

We thank the RBC and UKQCD collaborations for providing us their domain wall fermion gauge configurations. Y. Y. is supported by the US National Science Foundation under Grant No. PHY 1653405 "CAREER: Constraining Parton Distribution Functions for New-Physics Searches." Y. C. and Z. L. acknowledge the support of the National Science Foundation of China under Grants No. 11575196, No. 11575197, and No. 11335001. This work is partially supported by DOE Grant No. DE-SC0013065 and by the DOE TMD topical collaboration. This research used resources of the Oak Ridge Leadership Computing Facility at the Oak Ridge National Laboratory, which is supported by the Office of Science of the U.S. Department of Energy under Contract No. DE-AC05-00OR22725. This work used Stampede time under the Extreme Science and Engineering Discovery Environment (XSEDE), which is supported by National Science Foundation Grant No. ACI-1053575. We also thank the National Energy Research Scientific Computing Center (NERSC) for providing HPC resources that have contributed to the research results reported within this Letter. We acknowledge the facilities of the USQCD Collaboration used for this research in part, which are funded by the Office of Science of the U.S. Department of Energy.

[1] X.-D. Ji, Phys. Rev. Lett. **74**, 1071 (1995).
[2] Y.-B. Yang, Y. Chen, T. Draper, M. Gong, K.-F. Liu, Z. Liu, and J.-P. Ma, Phys. Rev. D **91**, 074516 (2015).
[3] S. Caracciolo, G. Curci, P. Menotti, and A. Pelissetto, Ann. Phys. (N.Y.) **197**, 119 (1990).
[4] Y.-B. Yang, A. Alexandru, T. Draper, J. Liang, and K.-F. Liu (χQCD Collaboration), Phys. Rev. D **94**, 054503 (2016).
[5] Y. Aoki *et al.* (RBC and UKQCD Collaborations), Phys. Rev. D **83**, 074508 (2011).
[6] T. Blum *et al.* (RBC and UKQCD Collaborations), Phys. Rev. D **93**, 074505 (2016).
[7] R. S. Sufian, Y.-B. Yang, A. Alexandru, T. Draper, J. Liang, and K.-F. Liu, Phys. Rev. Lett. **118**, 042001 (2017).
[8] T.-W. Chiu, Phys. Rev. D **60**, 034503 (1999).
[9] K.-F. Liu, Int. J. Mod. Phys. **A20**, 7241 (2005).
[10] T.-W. Chiu and S. V. Zenkin, Phys. Rev. D **59**, 074501 (1999).
[11] A. Li *et al.* (χQCD Collaboration), Phys. Rev. D **82**, 114501 (2010).
[12] M. Gong *et al.* (χQCD Collaboration), Phys. Rev. D **88**, 014503 (2013).
[13] Y.-B. Yang, A. Alexandru, T. Draper, M. Gong, and K.-F. Liu, Phys. Rev. D **93**, 034503 (2016).
[14] A. Hasenfratzand F. Knechtli, Phys. Rev. D **64**, 034504 (2001).
[15] J. Liang, Y.-B. Yang, K.-F. Liu, A. Alexandru, T. Draper, and R. S. Sufian, Phys. Rev. D **96**, 034519 (2017).
[16] B. C. Tiburzi, Phys. Rev. D **72**, 094501 (2005); **79**, 039904(E) (2009).
[17] C. Patrignani *et al.* (Particle Data Group), Chin. Phys. C **40**, 100001 (2016).
[18] R. Horsley, R. Millo, Y. Nakamura, H. Perlt, D. Pleiter, P. E. L. Rakow, G. Schierholz, A. Schiller, F. Winter, and J. M. Zanotti (UKQCD, QCDSF), Phys. Lett. B **714**, 312 (2012).
[19] Y.-B. Yang, R. S. Sufian, A. Alexandru, T. Draper, M. J. Glatzmaier, K.-F. Liu, and Y. Zhao, Phys. Rev. Lett. **118**, 102001 (2017).

[20] K.-F. Liu, J. Liang, and Y.-B. Yang, Phys. Rev. D **97**, 034507 (2018).
[21] Y.-B. Yang, M. Gong, J. Liang, H.-W. Lin, K.-F. Liu, D. Pefkou, and P. Shanahan, arXiv:1805.00531.
[22] J. A. Gracey, Nucl. Phys. **B667**, 242 (2003).
[23] Y.-B. Yang, M. Glatzmaier, K.-F. Liu, and Y. Zhao, arXiv:1612.02855.
[24] See Supplemental Material at http://link.aps.org/supplemental/10.1103/PhysRevLett.121.212001 for the details of the calculation and error estimation of the nonperturbative renormalization of the quark and glue energy momentum tensor.
[25] C. Alexandrou, M. Constantinou, T. Korzec, H. Panagopoulos, and F. Stylianou, Phys. Rev. D **83**, 014503 (2011).
[26] Z. Liu, Y. Chen, S.-J. Dong, M. Glatzmaier, M. Gong, A. Li, K.-F. Liu, Y.-B. Yang, and J.-B. Zhang (χQCD Collaboration), Phys. Rev. D **90**, 034505 (2014).
[27] Y. Bi, H. Cai, Y. Chen, M. Gong, K.-F. Liu, Z. Liu, and Y.-B. Yang, Phys. Rev. D **97**, 094501 (2018).
[28] S. Dulat, T.-J. Hou, J. Gao, M. Guzzi, J. Huston, P. Nadolsky, J. Pumplin, C. Schmidt, D. Stump, and C. P. Yuan, Phys. Rev. D **93**, 033006 (2016).
[29] L. A. Harland-Lang, A. D. Martin, P. Motylinski, and R. S. Thorne, Eur. Phys. J. C **75**, 204 (2015).
[30] H. Abramowicz *et al.* (ZEUS and H1 Collaborations), Eur. Phys. J. C **75**, 580 (2015).
[31] A. Accardi, L. T. Brady, W. Melnitchouk, J. F. Owens, and N. Sato, Phys. Rev. D **93**, 114017 (2016).
[32] S. Alekhin, J. Blümlein, S. Moch, and R. Placakyte, Phys. Rev. D **96**, 014011 (2017).
[33] R. D. Ball *et al.* (NNPDF Collaboration), Eur. Phys. J. C **77**, 663 (2017).
[34] H.-W. Lin *et al.*, Prog. Part. Nucl. Phys. **100**, 107 (2018).